

Multi-Shot Quantum Sensing for RF Signal Detection with MIMO Rydberg-Atom Receivers

Saman Atapattu*, Harini Hapuarachchi†, and Nathan Ross‡

*Department of Electrical and Electronic Engineering, School of Engineering, RMIT University, Melbourne, Australia

†School of Electrical and Computer Engineering, University of Sydney, Sydney, Australia

‡School of Mathematics and Statistics, University of Melbourne, Melbourne, Australia

Email: *saman.atapattu@rmit.edu.au, †harini.hapuarachchi@sydney.edu.au, ‡nathan.ross@unimelb.edu.au

Abstract—Rydberg-atom quantum receivers (RAQRs) enable electric-field sensing with quantum-noise-limited performance, yet their optical readout provides only magnitude measurements whose fluctuations follow Rician statistics governed by atomic projection noise, optical shot noise, reference-field injection, and short coherence times. These non-Gaussian, phase-blind measurements invalidate classical single-shot RF detectors and necessitate multi-shot quantum sensing strategies. This work develops a physically consistent multi-shot statistical model for RAQRs and derives both the optimal genie-aided likelihood-ratio test (LRT) and a practical phase-averaged LRT that removes dependence on the unknown RF-field phase. Closed-form test statistics and thresholds are obtained for both detectors, and the limits imposed by finite quantum shots—due to atomic dephasing and measurement backaction—are explicitly quantified. A fully non-coherent energy detector is also analysed, with exact detection probability derived using noncentral chi-square models. Monte Carlo results show that only 5–10 quantum shots yield major gains: the phase-averaged LRT closely approaches the genie bound and RAQR detection markedly outperforms classical RF energy detection under comparable received power. The proposed framework provides the first unified statistical basis for multi-shot Rydberg-based weak-field detection and underscores the potential of RAQRs for quantum-enhanced signal detection.

Index Terms—Rydberg-atom quantum receivers (RAQRs), quantum RF sensing, multi-shot detection, likelihood-ratio test (LRT), energy detection, spectrum sensing, signal detection.

I. INTRODUCTION

Quantum RF sensors based on Rydberg atoms have emerged as a powerful platform for detecting ultra-weak electromagnetic fields, in some regimes surpassing classical receiver sensitivity [1], [2]. Unlike conventional front ends that rely on mixers and coherent downconversion, a Rydberg-atom quantum receiver (RAQR) directly maps incident RF fields onto optical transmission via electromagnetically induced transparency (EIT), enabling room-temperature, quantum-noise-limited readout [3], [4]. This quantum transduction enables femtowatt-level sensing and supports applications in covert communication, spectrum awareness, and non-invasive RF monitoring [5], [6]. RAQR measurements differ fundamentally from classical I/Q samples: each interrogation yields a single *magnitude-only* value whose fluctuations follow a Rician law [7] determined by atomic projection noise, optical shot noise, and the injected reference field [8], [9]. This non-Gaussian structure limits the effectiveness of classical single-shot detectors and motivates principled *multi-shot quantum sensing* frameworks that explicitly incorporate Rydberg readout statistics into detection theory [6], [8].

A. Related Work

Recent literature underscores the potential of RAQRs as a credible alternative to classical RF systems. Foundational surveys outline their principles and advantages in sensitivity and form factor [3], while subsequent works have developed more accurate end-to-end signal models and digital linearization techniques to manage their inherent nonlinearity [4], [10]. A significant research thrust addresses the core challenge of “magnitude-only” detection. For multiple-input-multiple-output (MIMO) communications, this has led to capacity-achieving precoding schemes [11] and specialized channel estimation algorithms [12]. In wireless sensing, phase-retrieval-based methods have been adapted for angle-of-arrival (AoA) estimation and multi-user detection [8], [13], with a notable demonstration of single-sensor AoA recovery via intravapor interference [14]. From a detection-theoretic perspective, [6] formulated constant false alarm rate (CFAR) detectors and likelihood-ratio tests (LRTs) for single-shot measurements, and an information-theoretic analysis confirmed that the RAQR’s immunity to thermal noise can offset the capacity loss from its phase-blind nature [9]. Parallel hardware innovations, such as high-sensitivity enhancement resonators [1], [2] and broadband magnetic tuning architectures [15], continue to push performance boundaries.

B. Contributions

While existing work has established models and single-shot detection methods for RAQRs, a statistical theory for *multi-shot* detection—which aggregates several quantum measurements to improve reliability—remains unexplored. Current approaches, even those based on LRTs, typically rely on single-shot thresholding [6], leaving the full sensing potential of RAQRs untapped. *This paper bridges that gap by developing a comprehensive detection framework for multi-shot RAQR measurements.* Our specific contributions are:

- **Exact Multi-Shot LRT:** We derive the first multi-shot likelihood-ratio test for RAQR magnitude measurements, formalizing the underlying product-Rician statistical structure that arises from atomic noise and reference.
- **Practical Phase-Averaged LRT:** For scenarios with unknown signal phases (e.g., phase-shift keying (PSK)), we develop an implementable detector that marginalizes over the phase uncertainty using Rician moments, resulting in an LRT that requires no explicit waveform knowledge.

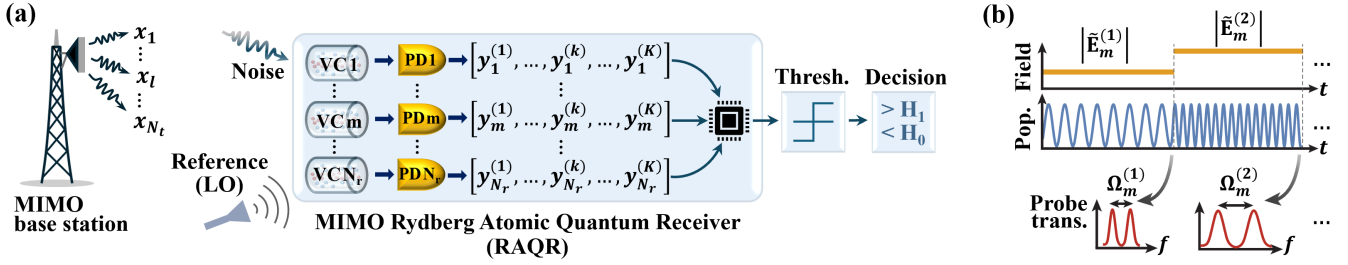


Fig. 1: (a) RF-quantum MIMO architecture in which a RAQR performs multi-shot optical readout. (b) Conceptual illustration of consecutive interrogation shots. For clarity, decoherence-induced damping of population oscillations is shown as negligible.

- *Non-Coherent Quantum Energy Detector (ED)*: We analyze an ED suitable when neither the channel nor the signal is known, and derive closed-form CFAR thresholds based on noncentral chi-square statistics.
- *Performance Analysis of Quantum Multi-Shot Gain*: Through numerical simulations, we demonstrate that aggregating a small number of shots ($K = 3-8$) yields significant performance gains. The proposed phase-averaged LRT recovers most of the performance of a genie-aided detector and substantially outperforms classical RF energy detectors operating at standard thermal noise levels.

This work establishes the first statistical framework for multi-shot quantum RF detection, highlighting its potential for quantum-enhanced spectrum sensing, weak-signal detection, and hybrid quantum-classical RF systems [16].

II. SYSTEM OVERVIEW

We consider a hybrid RF-quantum sensing scenario in which a multi-antenna primary transmitter communicates with its users while a secondary node monitors the spectrum using one or more Rydberg-atom quantum receivers (RAQRs). As shown in Fig. 1(a), the RAQR replaces the conventional RF front end and forms the first stage of a MIMO RF-quantum sensing architecture.

1) *Quantum Sensing Model*: A RAQR operates by mapping the incident RF field onto the optical response of a Rydberg atomic ensemble. Each interrogation produces a *magnitude-only* optical readout (Fig. 1(b)), whose fluctuations are dominated by atomic projection noise, photon shot noise, and the injected reference field rather than electronic thermal noise. Because each probe collapses the atomic state, only a limited number of measurements—typically a few to a few tens within the atomic coherence time—can be collected per sensing interval. These K magnitude samples from N_r vapor cells form the input to the multi-shot detectors developed here.

2) *Binary Detection Task*: The sensing objective is to determine whether an unknown RF emitter is present:

- \mathcal{H}_0 : reference field + quantum noise only,
- \mathcal{H}_1 : additional unknown RF field present.

Because the RAQR provides only noisy magnitudes, reliable discrimination requires aggregating multiple shots.

3) *Network Interpretation*: This model captures a range of wireless tasks: (i) spectrum sensing in cognitive radio; (ii) weak-emitter or unknown-signal detection; (iii) jammer or covert-transmitter identification; and (iv) interference monitoring in dense networks. In all cases, the RAQR acts as a quantum-enhanced front end that must infer emitter activity from a small set of non-Gaussian magnitude measurements.

4) *Role of Multi-Shot Processing*: Single-shot RAQR readouts are strongly noise-limited. Accumulating multiple interrogations stabilizes the underlying Rician statistics and enables reliable hypothesis testing. The detectors developed in this paper explicitly quantify performance as a function of the shot budget K and provide quantum-aware strategies that remain effective under realistic coherence-time constraints.

III. ANALYTICAL MODELS

Our objective is to develop a system and analytical framework that captures (i) the classical MIMO propagation from the primary base station (BS) and (ii) the quantum-optical measurement process inherent to the Rydberg-atom receiver. The remainder of this section establishes the models required for this joint RF-quantum sensing problem.

A. Network Model

We consider a primary MIMO transmitter with N_t collocated antennas and a secondary spectrum-sensing receiver equipped with N_r Rydberg-atom vapor cells (VCs), each coupled to an optical probe and photodetector, as shown in Fig. 1. A weak RF reference field, derived from a local oscillator (LO), is injected at each VC to stabilise the atomic response during measurement. The BS transmits an *unknown deterministic* constant-modulus vector

$$\mathbf{x} = [x_1, \dots, x_{N_t}]^T, \quad x_\ell = \sqrt{P_\ell} s_\ell, \quad (1)$$

where s_ℓ is a unit-modulus baseband symbol and P_ℓ is the per-antenna transmit power. The total transmit power satisfies $\|\mathbf{x}\|^2 = \sum_{\ell=1}^{N_t} |x_\ell|^2 = P$, and under constant-modulus signalling (e.g., M -PSK) this reduces to $\sum_{\ell=1}^{N_t} P_\ell = P$, with equal-power allocation $P_\ell = P/N_t$ commonly assumed.

The antennas operate at a carrier frequency resonant with the RF-driven Rydberg transition, and the radiated field propagates through a frequency-flat, quasistatic MIMO channel to the N_r VCs. Each VC performs K interrogation cycles—constituting a *multi-shot* measurement process (in con-

trast to the single-shot model of [6])—and produces K optical readouts that are jointly processed for spectrum sensing.

The total sensing duration $T_{\text{sig}} = KT_s$ is selected to lie within the channel coherence time, ensuring that the BS-to-VC channel remains approximately constant across all K shots.

B. Atom–Field Quantum Interaction

Each vapor cell (VC) contains an ensemble of alkali atoms prepared in a Rydberg configuration using two counter-propagating lasers: a weak probe beam driving the $|1\rangle \rightarrow |2\rangle$ transition and a strong coupling beam driving $|2\rangle \rightarrow |3\rangle$ [8], [17]. This establishes a ladder-type electromagnetically induced transparency (EIT) system whose upper state $|3\rangle$ is highly sensitive to incident RF fields. An RF field resonant with the $|3\rangle \leftrightarrow |4\rangle$ transition modifies the optical steady state through Autler–Townes (AT) splitting, and the corresponding change in probe transmission is recorded by the photodetector, yielding an estimate of the effective RF-driven Rabi frequency magnitude $\Omega_m^{(k)}$ during the k -th interrogation shot of VC m [8], [18]. The complex envelope of the RF field received at VC m during shot k is

$$\tilde{\mathbf{E}}_m^{(k)} = \frac{1}{2} \left(\sum_{\ell=1}^{N_t} \hat{\mathbf{e}}_{m,\ell} x_\ell \sqrt{\rho_{m,\ell}} g_{m,\ell} + \mathbf{R}_m + \mathbf{W}_{m,E}^{(k)} \right), \quad (2)$$

where $\rho_{m,\ell}$ denotes large-scale attenuation (assumed equal across ℓ , m due to the co-located geometry), $g_{m,\ell} \in \mathbb{C}$ models small-scale fading and RF phase, and $\hat{\mathbf{e}}_{m,\ell}$ is the polarization unit vector seen by VC m . The term \mathbf{R}_m is the received LO-derived reference field used to linearise and stabilise the atomic response, while $\mathbf{W}_{m,E}^{(k)}$ represents extrinsic free-space noise during shot k . Although the transmitted waveform and reference are constant across shots, each VC experiences a distinct spatially filtered version of the field due to its location, channel coefficients, and polarization coupling.

At the quantum level, the received field determines the magnitude of the Rabi coupling $\Omega_m^{(k)} \propto |\boldsymbol{\mu}_{34}^H \tilde{\mathbf{E}}_m^{(k)}|$, where $\boldsymbol{\mu}_{34}$ is the transition dipole moment. This Rabi frequency modulates the optical transparency, and the photodetected AT response produces the magnitude-only measurement used in our statistical model.

C. Multi-Shot Measurement

We assume that consecutive atomic interrogations are temporally separated such that the noise samples across shots are effectively uncorrelated. Each shot is taken only after the RF-driven Rabi-frequency magnitude $\Omega_m^{(k)}$ has reached a quasi-steady state within the shot duration T_s , as illustrated in Fig. 1(b). Under these constraints, the number of usable and approximately independent measurements within a signalling interval T_{sig} is limited by

$$K \lesssim \left\lfloor \frac{T_{\text{sig}}}{\max(T_R, T_N)} \right\rfloor, \quad (3)$$

where T_R denotes the AT-splitting (Rabi-magnitude) settling time and T_N denotes the noise correlation time determined by atomic and photon-shot fluctuations.

Experimental studies of room-temperature multi-photon Rydberg excitation show transient EIT/AT responses settling within a few microseconds [19]. The noise correlation time T_N is typically comparable to the atomic coherence time, which ranges from hundreds of nanoseconds to a few microseconds depending on the Rydberg level, vapor-cell temperature, and optical-beam configuration [20]. Thus, practical operating conditions often yield $T_R, T_N \sim 1\text{--}10 \mu\text{s}$.

Example: In a favourable room-temperature configuration with $T_N \sim 1\text{--}5 \mu\text{s}$ and $T_R \sim 2\text{--}10 \mu\text{s}$, a signalling block aligned with a typical wireless channel coherence interval of $T_c \approx 125 \mu\text{s}$ supports approximately $K \approx \left\lfloor \frac{T_c}{\max(T_R, T_N)} \right\rfloor \approx 10\text{--}12$ effectively independent measurement shots per vapor cell. These multi-shot observations form the basis of the statistical detection framework developed in this work.

D. Rabi-Frequency Mapping of the Received Field

Following the steady-state Rydberg–EIT/AT formalism in [8], [13], the stabilised atom–field coupling strength (i.e., Rabi-frequency magnitude) measured at the m -th vapor cell during the k -th interrogation is

$$\Omega_m^{(k)} = \left| \sum_{\ell=1}^{N_t} h_{m,\ell} x_\ell + r_m + w_{m,E}^{(k)} \right|, \quad (4)$$

where the effective complex channel gain $h_{m,\ell} = \frac{1}{\hbar} \boldsymbol{\mu}_{eg}^H \hat{\mathbf{e}}_{m,\ell} \sqrt{\rho_{m,\ell}} g_{m,\ell}$ captures the atomic dipole projection, RF-field polarization alignment, path loss, and small-scale fading, all assumed quasistatic over the signalling interval. The term $r_m = \boldsymbol{\mu}_{eg}^H \mathbf{R}_m / \hbar$ is the received component of the common LO reference field, while $w_{m,E}^{(k)} = \boldsymbol{\mu}_{eg}^H \mathbf{W}_{m,E}^{(k)} / \hbar \sim \mathcal{CN}(0, \sigma_{E,m}^2)$ denotes the projected extrinsic RF noise during the k -th shot. Under the deterministic signalling model introduced earlier, the transmitted symbols satisfy $x_\ell^{(k)} = x_\ell$ for all k , so only the projected noise term varies across shots. The mapping in (4) therefore provides a direct magnitude-only measurement of a coherent RF superposition plus noise and reference injection, as depicted in Fig. 1(b).

Both continuous-wave (CW) and pulsed multi-shot operation are compatible with (4). In a CW scheme, the probe and coupling beams remain on throughout the signalling interval, and the photodetector samples the AT splitting after the Rabi magnitude has stabilised within each shot duration T_s . In pulsed operation, the optical beams are re-applied for each shot, but the same steady-state expression applies provided that AT-splitting stabilisation is reached within T_s . In both cases, the statistical model of $\Omega_m^{(k)}$ is identical, differing only in the physical implementation of the measurement cycle.

E. Atomic Receiver Signal Model

Each Rydberg vapor cell produces a magnitude-only readout obtained from the steady-state Rabi frequency extracted via the probe transmission [8]. The measurement at the m -th cell during the k -th shot (Fig. 1) is modeled as

$$y_m^{(k)} = \left| \sum_{\ell=1}^{N_t} h_{m,\ell} x_\ell + r_m + w_m^{(k)} \right| = |[\mathbf{H}\mathbf{x}]_m + r_m + w_m^{(k)}| \quad (5)$$

where $[\mathbf{H}\mathbf{x}]_m$ is the m -th element of the received composite field. The full MIMO channel matrix is $\mathbf{H} = [h_{ij}] \in \mathbb{C}^{N_r \times N_t}$, where h_{ij} denotes the channel coefficient from transmit antenna j to receive antenna i . The transmit vector \mathbf{x} follows the unknown deterministic constant-modulus model in (1). The reference term r_m is the received component of the injected LO field. Stacking the noise across all shots yields

$$\mathbf{W} = [\mathbf{w}^{(1)}, \dots, \mathbf{w}^{(K)}], \quad \mathbf{w}^{(k)} \sim \mathcal{CN}(\mathbf{0}, \sigma_w^2 \mathbf{I}_{N_r}), \quad (6)$$

with entries $[\mathbf{W}]_{m,k} = w_m^{(k)} = w_{m,E}^{(k)} + w_{m,I}^{(k)}$. Here $w_{m,E}^{(k)}$ is projected RF/environmental noise and $w_{m,I}^{(k)}$ collects internal noise sources such as quantum projection noise, photon-shot noise, and electronics. Consistent with prior RAQR-based sensing models [6], [17], [21], we adopt the tractable and experimentally supported CSCG approximation $w_m^{(k)} \sim \mathcal{CN}(0, \sigma_w^2)$, where $\sigma_w^2 = \sigma_{E,m}^2 + \sigma_{I,m}^2$, with samples assumed i.i.d. across receivers and shots. Under this model, each RAQR output is a Rician-distributed magnitude of a coherent RF field plus quantum-dominated noise, greatly differing from classical coherent I/Q samples and forming the basis of the detection framework developed next.

F. Detection Problem Formulation

We consider a *multi-shot* sensing model in which each of the N_r Rydberg receivers produces K temporally independent magnitude measurements. As illustrated in Fig. 1(a), collecting all observations gives

$$\mathbf{Y} = \begin{bmatrix} y_1^{(1)} & \cdots & y_1^{(K)} \\ \vdots & \ddots & \vdots \\ y_{N_r}^{(1)} & \cdots & y_{N_r}^{(K)} \end{bmatrix} \in \mathbb{R}_+^{N_r \times K}.$$

The goal is to determine whether an unknown RF field is *absent* or *present*. Under the magnitude-only RAQR model (5), the binary hypothesis test becomes

$$\mathbf{Y} = \begin{cases} |\mathbf{R} + \mathbf{W}|, & \mathcal{H}_0 : \text{no RF signal,} \\ |\mathbf{H}\mathbf{X} + \mathbf{R} + \mathbf{W}|, & \mathcal{H}_1 : \text{RF signal present,} \end{cases} \quad (7)$$

where the block-structured quantities are

$$\mathbf{X} = \mathbf{x}\mathbf{1}_K^T, \quad \mathbf{R} = \mathbf{r}\mathbf{1}_K^T, \quad \mathbf{W} = [\mathbf{w}^{(1)}, \dots, \mathbf{w}^{(K)}],$$

and $|\cdot|$ denotes elementwise magnitude. The unknown deterministic vector $\mathbf{x} \in \mathbb{C}^{N_t}$ represents the BS transmission during the coherence interval; $\mathbf{r} \in \mathbb{C}^{N_r}$ is the received reference field; and $\mathbf{H} \in \mathbb{C}^{N_r \times N_t}$ is the quasistatic MIMO channel mapping the primary transmitter to the Rydberg sensors.

Temporal assumptions.: Throughout a wireless coherence block, the tuple $(\mathbf{H}, \mathbf{x}, \mathbf{r})$ remains constant. Shot-to-shot randomness originates solely from independent atomic and optical noise samples $[\mathbf{W}]_{m,k} = w_m^{(k)} \sim \mathcal{CN}(0, \sigma_w^2)$, for $m = 1 : N_r$, $k = 1 : K$, which are assumed i.i.d. across cells and shots. This model captures the physical constraints of RAQR operation: deterministic incident fields within a coherence interval, but independent quantum-limited fluctuations across interrogation shots. This multi-shot magnitude framework forms the basis for the likelihood-ratio derivations and detector designs presented in the following sections.

IV. MULTI-SHOT LIKELIHOOD RATIO TEST (LRT)

Quantum sensors such as Rydberg-atom receivers do not produce coherent I/Q samples; instead, each interrogation yields a noisy *magnitude-only* measurement whose statistics follow a Rician law shaped by atomic quantum noise, reference-field injection, and the shot-to-shot reset of the atomic ensemble. As a result, classical RF detection techniques—which rely on Gaussian baseband models—do not apply directly. This section establishes the likelihood functions associated with the multi-shot RAQR model and derives the corresponding LRTs that form the statistical foundation for quantum-enhanced RF detection.

From the multi-shot model in (7), each observation satisfies

$$y_m^{(k)} = \begin{cases} |r_m + w_m^{(k)}|, & \mathcal{H}_0, \\ |\mathbf{h}_m^T \mathbf{x} + r_m + w_m^{(k)}|, & \mathcal{H}_1, \end{cases} \quad k = 1, \dots, K, \quad (8)$$

where the noise samples $w_m^{(k)} \sim \mathcal{CN}(0, \sigma_w^2)$ are independent across vapor cells m and shots k .

A. Likelihood Functions

Under either hypothesis, the complex quantity inside the magnitude in (8) is Gaussian with mean $\mu_{m,0} = r_m$ under \mathcal{H}_0 and $\mu_{m,1} = \alpha_m(\mathbf{x}) \triangleq \mathbf{h}_m^T \mathbf{x} + r_m$ under \mathcal{H}_1 . Therefore each $y_m^{(k)}$ is Rician-distributed [7], and independence across (m, k) yields factored likelihoods.

Under \mathcal{H}_0 ,

$$p(\mathbf{Y}|\mathcal{H}_0) = \prod_{m=1}^{N_r} \prod_{k=1}^K \frac{y_m^{(k)}}{\sigma_w^2} I_0 \left(\frac{2y_m^{(k)} |r_m|}{\sigma_w^2} \right) e^{-\frac{(y_m^{(k)})^2 + |r_m|^2}{\sigma_w^2}}, \quad (9)$$

where $I_0(\cdot)$ is modified Bessel function of the first kind [22].

Under \mathcal{H}_1 ,

$$p(\mathbf{Y}|\mathcal{H}_1, \mathbf{x}) = \prod_{m=1}^{N_r} \prod_{k=1}^K \frac{y_m^{(k)}}{\sigma_w^2} I_0 \left(\frac{2y_m^{(k)} |\alpha_m(\mathbf{x})|}{\sigma_w^2} \right) \times e^{-\frac{(y_m^{(k)})^2 + |\alpha_m(\mathbf{x})|^2}{\sigma_w^2}}. \quad (10)$$

The likelihood-ratio test (LRT) is defined as [23]

$$\Lambda(\mathbf{Y}) = \frac{p(\mathbf{Y}|\mathcal{H}_1)}{p(\mathbf{Y}|\mathcal{H}_0)} \underset{\mathcal{H}_0}{\overset{\mathcal{H}_1}{\gtrless}} \eta, \quad (11)$$

where η is the MAP threshold determined by the prior probability $P(\mathcal{H}_1)$.

A central challenge is that the BS transmit vector \mathbf{x} is unknown to the RAQR. This motivates two detector classes:

- 1) *Genie-aided LRT*: assumes perfect knowledge of \mathbf{x} . This detector is not implementable but provides a fundamental quantum-sensing performance bound.
- 2) *Phase-averaged LRT (practical)*: exploits the constant-modulus structure of M -PSK signalling and replaces $|\alpha_m(\mathbf{x})|$ with its statistical expectation, yielding a computationally efficient detector.

These two LRTs provide (i) a quantum-limited benchmark and (ii) an implementable RAQR-specific detection strategy that respects the magnitude-only Rician measurement.

B. Genie-Aided LRT

For fixed $(\mathbf{H}, \mathbf{x}, \mathbf{r})$, each RAQR observation in (8) is Rician with noncentrality $|r_m|$ under \mathcal{H}_0 and $|\alpha_m|$, $\alpha_m = \mathbf{h}_m^T \mathbf{x} + r_m$, under \mathcal{H}_1 . Using (9)–(10), cancelling common factors, and taking logarithms gives the *exact* multi-shot log-likelihood ratio

$$\ln \Lambda(\mathbf{Y}) = \sum_{m=1}^{N_r} \sum_{k=1}^K \left[\frac{|r_m|^2 - |\alpha_m|^2}{\sigma_w^2} + \ln \frac{I_0\left(\frac{2y_m^{(k)}|\alpha_m|}{\sigma_w^2}\right)}{I_0\left(\frac{2y_m^{(k)}|r_m|}{\sigma_w^2}\right)} \right]. \quad (12)$$

This constitutes the optimal quantum-limited detector for the RAQR under the magnitude-only sensing model. Only the Bessel-ratio term depends on the observed data. The quadratic term $C_{GA} = \frac{K}{\sigma_w^2} \sum_{m=1}^{N_r} (|r_m|^2 - |\alpha_m|^2)$ is a deterministic offset for a fixed block. Moving it to the right-hand side yields the equivalent test

$$T_{GA}(\mathbf{Y}) = \sum_{m=1}^{N_r} \sum_{k=1}^K \ln \frac{I_0\left(\frac{2y_m^{(k)}|\alpha_m|}{\sigma_w^2}\right)}{I_0\left(\frac{2y_m^{(k)}|r_m|}{\sigma_w^2}\right)} \underset{\mathcal{H}_0}{\overset{\mathcal{H}_1}{\gtrless}} \tau^*, \quad (13)$$

with the normalized threshold

$$\tau_{GA}^* = \ln \eta - \frac{K}{\sigma_w^2} \sum_{m=1}^{N_r} (|r_m|^2 - |\alpha_m|^2). \quad (14)$$

This normalized form is used in simulations because it isolates all measurement-dependent contributions of the RAQR (i.e., the quantum Rician fluctuations) on the left, while absorbing the deterministic atomic-channel offset into a single threshold τ^* .

C. Phase-Averaged LRT

In practice, the transmit vector \mathbf{x} belongs to the primary system and is unknown to the RAQR-based sensing receiver. Under constant-modulus M -PSK signalling, $x_\ell = \sqrt{P_\ell} e^{j\theta_\ell}$ with θ_ℓ uniformly drawn from the PSK alphabet, the secondary receiver has no knowledge of the symbol phases. Hence the noncentrality parameter $|\alpha_m(\mathbf{x})| = |\mathbf{h}_m^T \mathbf{x} + r_m|$ in the genie-aided LRT (12) is unknown. A tractable approximation replaces $|\alpha_m(\mathbf{x})|$ with its phase-averaged value $\bar{\alpha}_m \triangleq \mathbb{E}_\theta [|\mathbf{h}_m^T \mathbf{x} + r_m|]$. Writing $v_m = \sum_{\ell=1}^{N_t} h_{m,\ell} \sqrt{P_\ell} e^{j\theta_\ell}$, so $\alpha_m = v_m + r_m$, the random phasor sum v_m is well approximated as $v_m \sim \mathcal{CN}(0, \sigma_{v,m}^2)$ with $\sigma_{v,m}^2 = \frac{P}{N_t} \sum_{\ell=1}^{N_t} |h_{m,\ell}|^2$, yielding the closed-form Rician mean $\bar{\alpha}_m = \mathbb{E}[|\alpha_m|]$ [7] as

$$\bar{\alpha}_m = \sqrt{\frac{\pi \sigma_{v,m}^2}{4}} L_{1/2} \left(-\frac{|r_m|^2}{\sigma_{v,m}^2} \right),$$

where $L_{1/2}(\cdot)$ is a Laguerre polynomial. Substituting $|\alpha_m| \rightarrow \bar{\alpha}_m$ in (12) gives the implementable phase-averaged LRT

$$\ln \Lambda(\mathbf{Y}) = \sum_{m=1}^{N_r} \sum_{k=1}^K \left[\frac{|r_m|^2 - \bar{\alpha}_m^2}{\sigma_w^2} + \ln \frac{I_0\left(\frac{2y_m^{(k)}\bar{\alpha}_m}{\sigma_w^2}\right)}{I_0\left(\frac{2y_m^{(k)}|r_m|}{\sigma_w^2}\right)} \right]. \quad (15)$$

As in the genie-aided case, the observation-independent term $C_{PA} = \frac{K}{\sigma_w^2} \sum_{m=1}^{N_r} (|r_m|^2 - \bar{\alpha}_m^2)$ is a deterministic block

offset. Moving it to the right-hand side yields the practical decision rule

$$T_{PA}(\mathbf{Y}) = \sum_{m=1}^{N_r} \sum_{k=1}^K \ln \frac{I_0\left(\frac{2y_m^{(k)}\bar{\alpha}_m}{\sigma_w^2}\right)}{I_0\left(\frac{2y_m^{(k)}|r_m|}{\sigma_w^2}\right)} \underset{\mathcal{H}_0}{\overset{\mathcal{H}_1}{\gtrless}} \tau_{PA}^*, \quad (16)$$

with the shifted threshold

$$\tau_{PA}^* = \ln \eta - \frac{K}{\sigma_w^2} \sum_{m=1}^{N_r} (|r_m|^2 - \bar{\alpha}_m^2). \quad (17)$$

The detector in (16) depends only on $(\mathbf{H}, \mathbf{r}, P)$ and thus provides a fully realizable quantum-aware LRT for RAQR sensing. It preserves the functional structure of the optimal genie-aided test, while eliminating dependence on the unknown—and rapidly varying—instantaneous symbol phases of the primary transmitter.

Remark 1 (Accuracy and Limitations of the Phase-Averaged LRT). *The phase-averaged approximation replaces the unknown noncentrality $|\mathbf{h}_m^T \mathbf{x} + r_m|$ with its statistical mean and is therefore implementable under realistic RAQR operation where the primary symbol phases are unknown and vary rapidly. Because the Rician likelihood depends on the magnitude of the complex mean—not its power—the approximation is inevitably looser than the genie-aided case, which uses the exact instantaneous value. Nevertheless, numerical results show that for multi-shot operation ($K \geq 5$), the phase-averaged LRT captures most of the achievable quantum-sensing gain, providing a physically consistent detector for practical RAQR-based spectrum monitoring.*

V. NON-COHERENT ENERGY DETECTOR (ED)

In many quantum-sensing scenarios, a Rydberg-atom receiver cannot rely on coherent MIMO information: the atomic ensemble does not provide access to the RF carrier phase, the BS transmit vector \mathbf{x} is unknown, and the channel matrix \mathbf{H} cannot be estimated from magnitude-only measurements. This motivates a fully *non-coherent* benchmark detector that uses only the total optical energy collected across vapor cells and shots.

The decision rule for energy detector statistic is [24]

$$T_{ED}(\mathbf{Y}) = \sum_{m=1}^{N_r} \sum_{k=1}^K (y_m^{(k)})^2 \underset{\mathcal{H}_0}{\overset{\mathcal{H}_1}{\gtrless}} \tau, \quad (18)$$

which denotes the accumulated optical energy.

1) *Distribution under \mathcal{H}_0 and \mathcal{H}_1* : Each magnitude measurement satisfies $y_m^{(k)} = |\nu_{i,m} + w_m^{(k)}|$ with $i \in \{0, 1\}$, where $w_m^{(k)} \sim \mathcal{CN}(0, \sigma_w^2)$ and $\nu_{0,m} = r_m$, $\nu_{1,m} = \mathbf{h}_m^T \mathbf{x} + r_m$. Thus,

$$\frac{2}{\sigma_w^2} (y_m^{(k)})^2 \sim \chi_2^2(\lambda_{i,m}), \quad \lambda_{i,m} = \frac{2|\nu_{i,m}|^2}{\sigma_w^2}.$$

Summing over $L = N_r K$ independent terms gives

$$Z \triangleq \frac{2}{\sigma_w^2} T_{ED} \sim \chi_{2L}^2(\Lambda_i), \quad \Lambda_i = K \sum_{m=1}^{N_r} \lambda_{i,m}.$$

2) *Exact CFAR Threshold and Detection Probability:*

Under \mathcal{H}_0 , the test statistic $Z \triangleq \frac{2}{\sigma_w^2} T_{\text{ED}}$ follows a noncentral chi-square distribution $Z \sim \chi_{2L}^2(\Lambda_0)$ with $L = N_r K$ degrees of freedom. Hence the false-alarm probability is

$$P_{\text{FA}} = \Pr(Z > z_\tau \mid \mathcal{H}_0) = Q_L\left(\sqrt{\Lambda_0}, \sqrt{z_\tau}\right), \quad z_\tau = \frac{2\tau}{\sigma_w^2}, \quad (19)$$

where $Q_L(\cdot, \cdot)$ denotes the generalized Marcum- Q function [25]. Since the secondary node lacks channel or waveform knowledge, it is reasonable to operate the ED under a fixed CFAR level P_{FA} . Solving (19) for the threshold gives

$$\tau = \frac{\sigma_w^2}{2} \left[Q_L^{-1}(P_{\text{FA}}; \sqrt{\Lambda_0}) \right]^2. \quad (20)$$

Under \mathcal{H}_1 , the noncentrality parameter becomes Λ_1 , yielding

$$P_{\text{D}} = \Pr(Z > z_\tau \mid \mathcal{H}_0) = Q_L\left(\sqrt{\Lambda_1}, \sqrt{z_\tau}\right). \quad (21)$$

Substituting the CFAR threshold (20) into (21) produces the closed-form CFAR detection probability

$$P_{\text{D}}(P_{\text{FA}}) = Q_L\left(\sqrt{\Lambda_1}, Q_L^{-1}(P_{\text{FA}}; \sqrt{\Lambda_0})\right). \quad (22)$$

Remark 2 (Role and Limitations of the Non-Coherent ED). *The non-coherent ED uses only total optical energy and discards all quantum-spatial structure of the RAQR. It does not exploit the coherent MIMO combining inherent in $\mathbf{H}\mathbf{x}$, nor the nonlinear Rydberg response encoded in the Rician likelihood. As such, it provides a deliberately conservative baseline for quantum sensing: simple, physically robust, and implementable when the atomic receiver cannot track phase or estimate the RF channel, but significantly suboptimal compared with the LRT-based detectors that leverage RAQR physics.*

3) *Classical RF Energy Detector (Baseline for Comparison):* To quantify the sensing advantage of Rydberg-atom receivers, we compare against the *classical RF energy detector*, which represents the standard non-coherent baseline used in spectrum sensing, radar, and low-SNR emitter detection. Unlike the RAQR, the RF receiver acquires coherent complex baseband samples, has no reference-field injection, and operates under thermal-noise-limited statistics. This contrast isolates the benefit of the RAQR's quantum noise floor and reference-assisted magnitude readout.

RF Observation Model: The m -th RF sensor collects K_{RF} complex baseband samples,

$$y_m^{(k)} = \begin{cases} n_m^{(k)}, & \mathcal{H}_0, \\ \mathbf{g}_m^T \mathbf{x} + n_m^{(k)}, & \mathcal{H}_1, \end{cases} \quad k = 1, \dots, K_{\text{RF}},$$

where $n_m^{(k)} \sim \mathcal{CN}(0, \sigma_n^2)$ i.i.d. across m, k , and $\mathbf{g}_m \in \mathbb{C}^{N_t \times 1}$ is the RF channel to sensor m , distinct from the quantum-channel vector \mathbf{h}_m used by the RAQR. The deterministic signal term under \mathcal{H}_1 is $\mu_m \triangleq \mathbf{g}_m^T \mathbf{x}$, where \mathbf{x} is the same (unknown) transmit vector seen by both the RF and RAQR receivers.

Non-Coherent RF Energy Detector: The RF energy detector forms the statistic

$$T_{\text{ED}}^{(\text{RF})} = \sum_{m=1}^{N_r} \sum_{k=1}^{K_{\text{RF}}} |y_m^{(k)}|^2 \underset{\mathcal{H}_0}{\overset{\mathcal{H}_1}{\geq}} \tau_{\text{RF}}, \quad (23)$$

where τ_{RF} is the threshold. Define the normalized test variable $Z_{\text{RF}} \triangleq \frac{2}{\sigma_n^2} T_{\text{ED}}^{(\text{RF})}$ with $L = N_r K_{\text{RF}}$.

Distribution under \mathcal{H}_0 . When $y_m^{(k)} = n_m^{(k)}$, the statistic satisfies $Z_{\text{RF}} \mid \mathcal{H}_0 \sim \chi_{2L}^2$, so the false-alarm probability is

$$P_{\text{FA}} = Q_L(0, \sqrt{z_\tau}), \quad z_\tau = \frac{2\tau_{\text{RF}}}{\sigma_n^2}, \quad (24)$$

where $Q_L(\cdot, \cdot)$ is the generalized Marcum- Q function.

Distribution under \mathcal{H}_1 . Under \mathcal{H}_1 , each sample has mean μ_m , giving $Z_{\text{RF}} \mid \mathcal{H}_1 \sim \chi_{2L}^2(\Lambda_{\text{RF}})$, with aggregate noncentrality parameter

$$\Lambda_{\text{RF}} = \sum_{m=1}^{N_r} \frac{2K_{\text{RF}} |\mu_m|^2}{\sigma_n^2} = \frac{2K_{\text{RF}}}{\sigma_n^2} \sum_{m=1}^{N_r} |\mathbf{g}_m^T \mathbf{x}|^2. \quad (25)$$

Hence the detection probability is

$$P_{\text{D}} = Q_L\left(\sqrt{\Lambda_{\text{RF}}}, \sqrt{z_\tau}\right), \quad (26)$$

which serves as the classical baseline against which RAQR performance is evaluated.

Remark 3 (RAQR vs. RF Energy Detection). *Classical RF receivers rely on coherent I/Q sampling and thermal-noise-limited statistics, enabling arbitrarily large sample counts and asymptotic detection gains. In contrast, a Rydberg-atom quantum receiver operates in the quantum-optical regime: its measurements are magnitude-only, Rician distributed, and constrained by atomic coherence times, allowing only a limited number of independent shots. Despite this restriction, the RAQR benefits from a much lower intrinsic noise floor and reference-assisted field readout, enabling reliable weak-signal detection with far fewer samples than required by an RF front end. Thus, the RF ED serves as a classical baseline, while the RAQR ED reveals the fundamental sensing advantage arising from quantum-enabled field extraction.*

VI. NUMERICAL RESULTS

We now evaluate the performance of the proposed multi-shot RAQR detectors. Unless otherwise stated, the system employs $N_t = 3$ transmit antennas and $N_r = 4$ vapor-cell receivers with deterministic 4-PSK signalling. The carrier frequency is set to 28 GHz and is matched to the Rydberg transition $62D_{5/2} \leftrightarrow 64P_{3/2}$, whose electric-dipole moment is $\boldsymbol{\mu}_{eg} = [0, 789.1 qa_0, 0]^T$ ($q = 1.602 \times 10^{-19}$ C, $a_0 = 5.292 \times 10^{-11}$ m). Quantum noise is modeled as $w_m^{(k)} \sim \mathcal{CN}(0, \sigma_w^2)$, corresponding to a thermal-equivalent noise floor of approximately -97 dBm over a ~ 1 MHz optical detection bandwidth. Channel coefficients $h_{m,\ell} \sim \mathcal{CN}(0, 1)$ are normalized to represent co-located Rydberg cells. The total transmit power P is chosen so that the effective sensing SNR is 0 dB based on the average Frobenius norm of \mathbf{H} . All results are averaged over 10^5 Monte Carlo realizations. We report

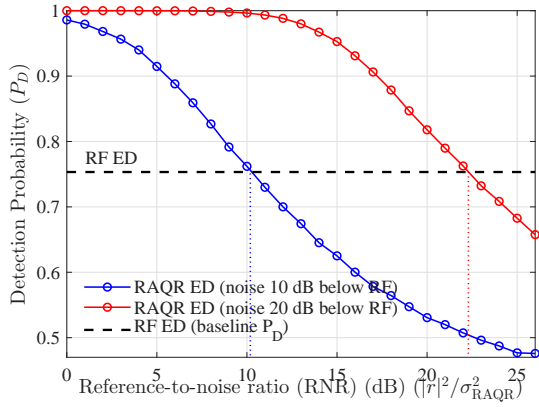


Fig. 2: Detection probability P_D versus reference-to-noise ratio (RNR) at CFAR $P_{FA} = 0.1$ for RAQR and RF EDs.

either the Bayesian total error probability $P_e = \frac{1}{2}(P_{FA} + P_{MD})$ with equal priors, or—under a CFAR design—the detection probability P_D at $P_{FA} = 0.1$.

Figure 2 shows the detection probability P_D at $P_{FA} = 0.1$ versus the reference-to-noise ratio $\text{RNR} = |r|^2 / \sigma_{w,\text{RAQR}}^2$. The RF energy detector exhibits a constant $P_D \approx 0.75$ since its central chi-square statistic is independent of any reference tone. In contrast, the RAQR statistic is noncentral (Rician), and its detectability varies with the reference amplitude. With a 10 dB RAQR noise advantage, the RAQR ED outperforms the RF ED for $\text{RNR} \lesssim 10$ dB; with a 20 dB advantage, the crossover increases to $\text{RNR} \approx 22$ dB. These trends highlight that RAQR performance is maximized when the injected reference is matched to its low intrinsic noise floor—overly strong references suppress the signal contribution and degrade detection.

Figure 3 compares blind RAQR and RF energy detectors under a CFAR constraint $P_{FA} = 0.1$. With only $K_{\text{RAQR}} = 5$ shots, the RAQR achieves $P_D \approx 0.95$ due to its low intrinsic noise floor and reference-induced noncentrality. An RF receiver with a 20 dB higher noise floor requires $K_{\text{RF}} \approx 20$ samples to reach comparable performance, whereas a 25 dB penalty pushes this requirement beyond $K_{\text{RF}} \approx 180$. These results show that, in the blind setting, RAQR achieves high detection probability with orders-of-magnitude fewer samples than a classical RF energy detector subject to a higher noise.

Figure 4a compares the ROC performance of the RAQR detectors for $K = 1$ and $K = 5$. The genie-aided LRT provides the fundamental bound; the phase-averaged LRT is the practical coherent detector; and the blind ED serves as the non-coherent baseline. At $P_{FA} = 0.1$, the phase-averaged LRT improves from $P_D \approx 0.5$ at $K = 1$ to $P_D \approx 0.85$ at $K = 5$, a $\sim 70\%$ relative gain. This ROC improvement highlights the role of multi-shot processing: single-shot RAQR measurements are heavily noise-limited, while a small number of repeats stabilizes the Rician statistics and markedly enhances hypothesis separability.

Figure 4b plots P_D versus the number of shots K under a CFAR constraint $P_{FA} = 0.1$. The genie-aided LRT provides the benchmark, reaching $P_D > 0.95$ by $K \approx 5$ and saturating

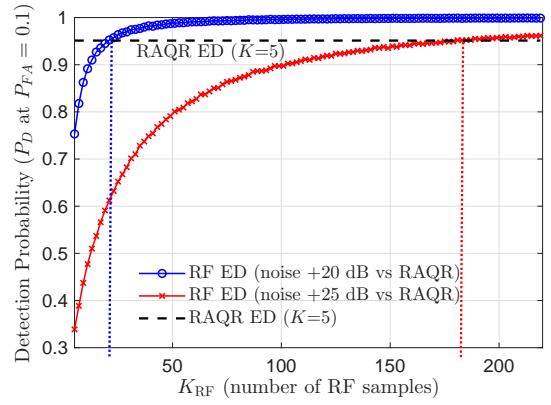


Fig. 3: Detection probability P_D versus number of RF samples K_{RF} at CFAR $P_{FA} = 0.1$. RAQR uses $K = 5$.

near unity for $K \geq 8$. The phase-averaged LRT increases steadily from $P_D \approx 0.48$ at $K = 1$ to $P_D \approx 0.94$ at $K = 12$, closely approaching the genie bound as K grows. The blind ED also improves with averaging but more slowly, rising from $P_D \approx 0.45$ at $K = 1$ to $P_D \approx 0.88$ at $K = 12$. These results show that the practical phase-averaged LRT captures most of the genie-aided performance with only a modest number of quantum shots, whereas the ED remains fundamentally constrained by its noncoherent nature.

Figure 4c shows the Bayesian total error versus the number of shots K . At $K = 1$, the genie, phase-averaged, and ED detectors achieve $P_e \approx 0.11$, 0.15 , and 0.19 , respectively. As K increases, the genie error drops fastest ($P_e \approx 2.8 \times 10^{-3}$ at $K = 5$ and 10^{-4} at $K = 10$), while the phase-averaged LRT decreases to $P_e \approx 2.7 \times 10^{-2}$ at $K = 5$ and 6×10^{-3} at $K = 10$. The ED improves only modestly and is limited by its noncoherent CFAR floor around 0.05. Overall, multi-shot processing is crucial for RAQR detection, and the phase-averaged LRT captures most of the genie gain while remaining fully implementable.

Remark 4 (Limits of Multi-Shot RAQR Acquisition). *Unlike RF receivers that can collect hundreds of independent samples per coherence interval, RAQRs support only a small number of usable shots ($K \lesssim 10$ – 20) before atomic backaction and collisional dynamics introduce temporal correlation. Beyond this regime, the i.i.d. Rician model breaks down and the likelihood becomes a correlated, non-Gaussian of magnitude-only measurements. Developing tractable detectors and statistical models for this correlated quantum readout regime remains an important open direction for future RAQR sensing theory.*

VII. CONCLUSION

This paper presented a unified statistical framework for multi-shot detection with Rydberg-atom quantum receivers. Using the magnitude-only optical readout imposed by atomic EIT, we derived the exact multi-shot LRT, a practical phase-averaged LRT that requires no knowledge of the unknown RF waveform, and a fully non-coherent energy detector with closed-form CFAR characterization. The analysis and simulations show that only a handful of quantum shots are sufficient

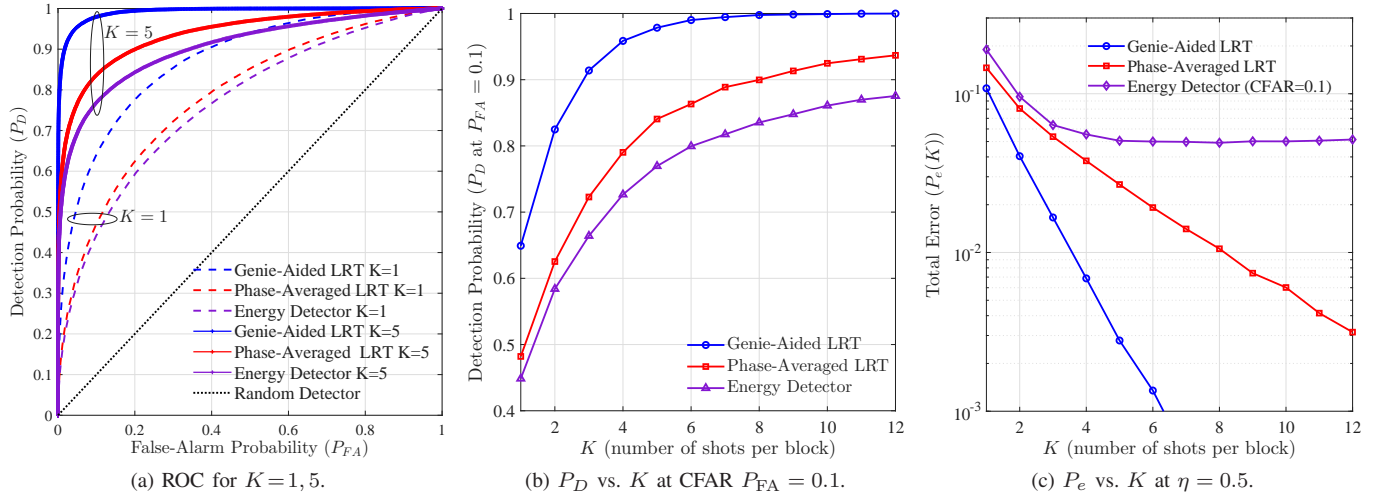


Fig. 4: Multi-shot RAQR detection performance. (a) ROC improvement with shot aggregation; (b) CFAR-constrained detection probability versus K ; (c) Bayesian total error versus K . The demonstrate that few-shot averaging provides large practical gains.

to stabilise the Rician measurement statistics, allowing the implementable phase-averaged LRT to approach genie-aided performance and substantially outperform classical RF energy detectors operating under realistic noise figures. These results demonstrate that multi-shot quantum processing is essential for unlocking the sensing capability of RAQRs and establish a rigorous bridge between quantum measurement constraints and classical detection theory. Future directions include modelling back-action-limited shot regimes, incorporating temporal noise correlations, extending the framework to wideband and multi-band RF fields, and exploring adaptive reference-field design. Such developments will further clarify the role of quantum receivers as front-end components in next-generation quantum-enhanced sensing for low-SNR RF systems.

REFERENCES

- [1] Y. Li, Y. Lin, Z. Ding, K. Yang, R. Ran, Z. Wan, and Y. Fu, "A compact tunable enhancement resonator for rydberg atomic receiver," *IEEE Antennas Wirel. Propag. Lett.*, vol. 24, no. 4, pp. 808–812, 2025.
- [2] W. Wan, et al., "Deep-subwavelength resonator based rydberg atomic receiver for HF band enhanced sensing," *IEEE Antennas Wirel. Propag. Lett.*, vol. 25, no. 1, pp. 19–23, 2025.
- [3] M. Cui, Q. Zeng, and K. Huang, "Rydberg atomic receiver: Next frontier of wireless communications," *IEEE Commun. Mag.*, vol. 64, no. 1, pp. 146–152, 2025.
- [4] T. Gong, et al., "An equivalent baseband signal model for rydberg atomic quantum receiver aided wireless communications and sensing," in *Proc. IEEE Int. Conf. on Quantum Communications, Networking, and Computing (QCNC)*, 2025, pp. 200–204.
- [5] M. Guo, Y. Guo, X. Guo, C. Guo, and Y. Wang, "Ultra-high precision LEO doppler localization facilitated by rydberg atomic receivers," *IEEE Trans. Veh. Technol.*, 2025.
- [6] S. Atapattu, N. Ross, and H. Hapuarachchi, "Detection of unknown RF signals using Rydberg-atom quantum MIMO receivers," *IEEE Commun. Lett.*, vol. 29, no. 10, pp. 2446–2450, 2025.
- [7] S. O. Rice, "Statistical properties of a sine wave plus random noise," *The Bell System Technical Journal*, vol. 27, no. 1, pp. 109–157, 1948.
- [8] M. Cui, Q. Zeng, and K. Huang, "Towards atomic MIMO receivers," *IEEE J. Select. Areas Commun.*, vol. 43, no. 3, pp. 659–673, 2025.
- [9] Y. Guo, X. Guo, Y. Wang, M. D. Renzo, and P. Zhang, "High SNR at a cost: The information-theoretic dilemma of magnitude-only atomic receivers," *IEEE Wireless Commun. Lett.*, vol. 14, no. 12, pp. 3997–4001, 2025.
- [10] Y. Xia, M.-M. Zhao, M. Li, M. Lei, and M. Zhao, "Digital nonlinear distortion compensation for rydberg atomic receiver with quadrature amplitude modulation," in *Int. Conf. Wireless Commun. Signal Process. (WCSP)*, 2024, pp. 697–702.
- [11] M. Cui, Q. Zeng, and K. Huang, "MIMO precoding for rydberg atomic receivers enabled wireless communications," in *Proc. IEEE Int. Conf. Commun. (ICC)*, 2025, pp. 4792–4797.
- [12] B. Xu, J. Zhang, Z. Chen, B. Cheng, Z. Liu, Y.-C. Wu, and B. Ai, "Channel estimation for rydberg atomic receivers," *IEEE Wireless Commun. Lett.*, vol. 14, no. 9, pp. 2957–2961, 2025.
- [13] H. Kim, H. Park, and S. Kim, "Quantum-MUSIC: Multiple signal classification for quantum wireless sensing," *IEEE Wireless Commun. Lett.*, vol. 14, no. 6, pp. 1623–1627, 2025.
- [14] Y. Guo, X. Guo, Y. Wang, M. D. Renzo, and P. Zhang, "AoA detection using a single rydberg atomic receiver: Leveraging inner-vapor interference," *IEEE Trans. Commun.*, vol. 73, no. 12, pp. 14 828–14 844, 2025.
- [15] W. Qimeng, Q. An, and Y. Fu, "Instantaneous bandwidth expansion of a gradient magnetic field-enhanced rydberg atomic receiver," *IEEE Sensors Journal*, vol. 25, no. 13, pp. 24 045–24 051, 2025.
- [16] A. Obando, S. Atapattu, P. Dharmawansa, A. Hourani, and K. Sithamparamanathan, "Eigenvalue-based detection in MIMO systems for integrated sensing and communication," in *Proc. IEEE Vehicular Technology Conf. (VTC2025-Fall)*, Chengdu, China, 2025.
- [17] T. Gong, A. Chandra, C. Yuen, Y. L. Guan, R. Dumke, C. M. S. See, M. Debbah, and L. Hanzo, "Rydberg atomic quantum receivers for classical wireless communication and sensing," *IEEE Wireless Commun.*, vol. 32, no. 5, pp. 90–100, 2025.
- [18] C. T. Fancher, D. R. Scherer, M. C. S. John, and B. L. S. Marlow, "Rydberg atom electric field sensors for communications and sensing," *IEEE Trans. Quantum Eng.*, vol. 2, pp. 1–13, 2021.
- [19] S. M. Bohachuk, F. Ripka, V. Venu, F. Christaller, C. Liu, M. Schmidt, H. Kübler, and J. P. Shaffer, "Three-photon rydberg-atom-based radio-frequency sensing scheme with narrow linewidth," *Physical Review Applied*, vol. 20, no. 6, p. L061004, 2023.
- [20] C. S. Adams, J. D. Pritchard, and J. P. Shaffer, "Rydberg atom quantum technologies," *Journal of Physics B: Atomic, Molecular and Optical Physics*, vol. 53, no. 1, p. 012002, 2019.
- [21] H. Kim, H. Park, J. Won, and S. Kim, "Multi-band quantum wireless sensing for rydberg atomic receivers," *IEEE Commun. Lett.*, vol. 29, no. 6, pp. 1476–1480, 2025.
- [22] I. S. Gradshteyn and I. M. Ryzhik, *Table of Integrals, Series, and Products*. Academic press, 2014.
- [23] H. L. V. Trees, *Detection, Estimation, and Modulation Theory*. New York Chichester: Wiley, 2001.
- [24] S. Atapattu, C. Tellambura, and H. Jiang, *Energy detection for spectrum sensing in cognitive radio*. Springer, 2014, vol. 6.
- [25] A. Nuttall, "Some integrals involving the Q_M function (corresp.)," *IEEE Trans. Inform. Theory*, vol. 21, no. 1, pp. 95–96, 1975.